Ab Initio Study of Radical Addition Reactions: Addition of a Primary Ethylbenzene Radical to Ethene (I)

V. Van Speybroeck,* D. Van Neck, and M. Waroquier

Laboratory of Theoretical Physics, Universiteit Gent, Proeftuinstraat 86, B-9000 Gent, Belgium

S. Wauters, M. Saeys, and G. B. Marin

Laboratorium voor Petrochemische Techniek, Universiteit Gent, Krijgslaan 281-S5, B-9000 Gent, Belgium

Received: June 16, 2000; In Final Form: August 29, 2000

Ab initio density functional theory calculations have been carried out on a model reaction involved in coke formation during the thermal cracking of hydrocarbons, namely, the addition of the ethylbenzene radical to ethene. This study enables one to get more microscopic insight into the mechanistic and kinetic aspects of the reaction. A profound ab initio conformational analysis of the formed products, reactants, and transition states is made. The impact of internal rotations on the two kinetic parameters deduced from transition state theory (TST), the activation energy and the preexponential factor, has been studied in detail. Furthermore, we report on the various components that govern the kinetic parameters. Preexponential factors are very sensitive to the accuracy of constructing the microscopic partition functions. Internal rotations play a dominant role in the reaction mechanism, and their impact on the preexponential factor is large. Hence, a very accurate handling of internal rotations is of crucial importance. We present a new algorithm to extract exactly on a quantum mechanical basis the partition functions of the internal rotations. The calculations as presented here are especially important for complex reaction schemes, for which experimental data are not always available.

1. Introduction

Thermal cracking of hydrocarbons is one of the main processes in the production of olefins. During the thermal cracking, a carbonaceous deposit, coke, is formed on the inner walls of the reactor tubes. This coke layer exhibits a negative influence on the efficiency of a cracking unit. Detailed models of elementary reactions for the thermal cracking[1] and semiempirical models for coke formation[2,3] are available. Thermal cracking proceeds via a radical mechanism; small radicals are formed via C−C bond breaking and react with the feed components via abstraction and addition reactions. Decomposition of the formed radical results in the desired gas-phase olefins. Radicals of the gas phase create radical species on the coke surface at which olefins can add. Cyclization and dehydrogenation lead to a further growth of the coke layer by incorporation of the carbon atoms. A major difficulty in developing detailed models is obtaining information on the kinetic and mechanistic aspects of elementary reactions and assessing the relative importance of competing pathways.

Because of the increasing capabilities of computers and optimization of currently available numerical methods, theoretical calculations on industrially important processes become feasible. A possible way to obtain accurate rate coefficients is through transition state theory.[4−8] This approach has been successfully used to obtain semiquantitative predictions for the preexponential factor and activation energies of gas-phase reactions.[9,10] The structure of the transition state was based on chemical intuition. Early attempts to develop a model for the frequency factor used empirical parameters such as entropic group contributions.[11] Although such models can be used for some qualitative predictions, their empirical origin limits their use for quantitative microscopic predictions.

Recently, ab initio calculations have been carried out to calculate accurate activation energies and frequency factors within the framework of transition state theory for the addition of *n*-alkyl radicals to ethene.[12−14]

In this paper, standard ab initio density functional theory (DFT) calculations were performed to analyze in detail the theoretical predictions concerning the addition of a primary ethylbenzene radical to ethene, the gas-phase analogue for one of the main reactions from the coke formation network, as schematically shown in Figure 1. This reaction is taken as a model reaction to outline the theoretical procedures concerning this type of calculation. Future work is aimed at applying these methods to other reactions of competing pathways in order to validate some basic assumptions made in the coke formation network.

Our study includes a detailed conformational analysis of the formed products and reactants in order to locate possible transition states and to get insight into different pathways toward reaction. Also, a detailed study of vibrational frequencies of the different species is presented. Some of the low-frequency modes are replaced by appropriate internal rotations to better model the partition functions required for the determination of the frequency factor. Internal rotations get special attention in this work, because these modes are better described by a hindered rotor model than by a harmonic oscillator model. To reduce the numerical complexity of dealing with coupled multidimensional rotors within manageable limits, we decouple the multidimensional Schrödinger equation in appropriate one-dimensional eigenvalue equations. The second-order differential

* To whom all correspondence should be addressed. Fax: 32 (0)9 264 65 42. E-mail: veronique.vanspeybroeck@rug.ac.be.

10.1021/jp002172o CCC: $19.00
Published on Web 10/21/2000

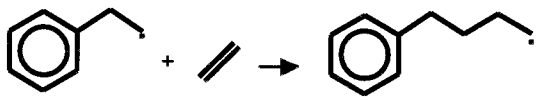

Figure 1. The addition of the primary ethylbenzene radical to ethene.

equation for each torsional angle is then solved via a new elegant numerical algorithm, as presented in the Appendix.

The microscopic partition functions are related to macroscopic quantities such as preexponential factors, activation barriers, and reaction rates by means of transition state theory (TST),[4,5] which has proved its success in many studies for the quantitative prediction of kinetic parameters.[6,7]

A detailed study is made on the rate of the reaction under discussion and on the role of internal rotations on the two Arrhenius parameters. In section 2, a brief overview of the applied theoretical methods is given, followed by a description of the computational details of the calculations in section 3. In the next sections, the results are presented and discussed and finally some conclusions are made.

2. Brief Overview of Theoretical Methods

The evaluation of macroscopic kinetic quantities such as the rate coefficient of a chemical reaction would in principle require the calculation of a large number of trajectories to create an appropriate ensemble (canonical, microcanonical, etc.). An averaging over all trajectories would then yield the required statistical quantities. For a better understanding of the reaction mechanism, one needs a microscopic approach. This microscopic treatment requires the instantaneous evaluation of the potential energy surface in a fully ab initio quantum mechanical way at each step on the trajectory of the reaction. Taking into consideration the number of different configurations that should be calculated with the computationally very expensive ab initio methods, this way of deriving macroscopic quantities on a fully microscopic basis becomes prohibitive.

It is in this field of relating macroscopic concepts of chemical reactions with the microscopic picture of internal reorganization of the individual molecules that TST has made a decisive contribution.[4−8] The partition functions constructed on a quantum mechanical basis serve as a bridge to the thermodynamic macroscopic properties of the system. The concept of TST relies on the static structure properties of three distinct states of the system: the reactants, the products, and the transition state. Although rather old in concept, the fundamental ideas of TST are still commonly used in chemical kinetics. Enormous progress is made in the microscopic description of the three relevant states, manifesting in a more reliable reproduction of the partition functions. Within TST, the rate equation for a bimolecular reaction A + B → C is given by[6,7]

$$k(T) = \frac{k_B T}{h} K_C^{\ddagger} \tag{1}$$

$$\text{with } K_C^{\ddagger} = \frac{q_{\ddagger}}{q_A q_B} e^{-\Delta E_0/(k_B T)} \tag{2}$$

The rate constant is expressed per unit volume, per molecule, and per time unit. k_B represents the Boltzmann constant. T stands for the temperature, and h is Planck's constant. The modified equilibrium constant, $K_C^{\ddagger}$, is microscopically completely determined by the global partition functions of the reactants and transition state. ΔE_0 represents the molecular energy difference at absolute zero between the activated complex and reactants (determined in Hartree−Fock (HF) or DFT). The zero-point energies of the various vibrational modes are also taken up in ΔE_0.

The partition functions q_A, q_B, and $q_{\ddagger}$ figuring in the equilibrium constant (eq 2) are factorized in the diverse degrees of freedom:

(1) The translational partition function is approximated by the familiar expression for ideal gases.[7]

(2) The rotational partition function (corresponding with the rotation of the global rigid molecule) is approached by some common expression.[6,7]

(3) The partition functions for the remaining $3N - 6$ vibrational modes (in a nonlinear molecule with N atoms) are evaluated within the harmonic oscillator approximation. Each normal mode with vibrational frequency ν_i has a partition function of the form

$$q_{\text{vib},i} = \frac{1}{1 - e^{-h\nu_i/(k_B T)}} \tag{3}$$

apart from the zero-point energy contribution $e^{-h\nu_i/(2k_B T)}$ which is taken up in ΔE_0, as already mentioned.

By analyzing the vibrational spectrum of the molecule and in particular the low vibrational modes, it is possible to identify some motions that correspond to internal rotations. Internal rotations correspond with rotations of one part of the molecule with respect to another about a single bond which is not part of a cyclic structure. The internal rotations are free or hindered depending on the presence of structural features inhibiting the rotation. An exact quantum mechanical treatment of the internal rotations is not feasible. All internal rotations are coupled with each other and with the instantaneous rotation of the rigid body. To reduce the analytical and computational cost within manageable limits, all internal rotations are decoupled but for the rotational potential energy which remains multidimensional in all torsional angles. This approach is commonly accepted, and one may expect that the omitted coupled terms only slightly affect the rotational energy spectra.[15,16]

Within this picture, the rotational wave function, ψ_{km}, for each internal rotation m is not only a function of the relevant torsional angle ϕ_m but also depends on the values of the $(M - 1)$ remaining torsional angles which are regarded as parameters. The energy levels are obtained by solving the following Schrödinger equation:[17,18]

$$-\frac{\hbar^2}{2I_m}\frac{\partial^2 \psi_{km}(\phi_1,\phi_2,...,\phi_M)}{\partial \phi_m^{\,2}} + V(\phi_1,\phi_2,...,\phi_M)\psi_{km}(\phi_1,\phi_2,...,\phi_M) = \epsilon_k(m)\psi_{km}(\phi_1,\phi_2,...,\phi_M) \quad \text{for} \quad m = 1, 2, ..., M \tag{4}$$

I_m is the reduced moment of inertia for the rotation of the mth top:

$$I_m = A_m\left(1 - \sum_{i=X,Y,Z} A_m \lambda_{mi}^{\,2}/I_i\right) \tag{5}$$

where A_m represents the moment of inertia of the mth top itself and λ_{mi} is the direction cosine between the axis of the mth top and the principal axis of the whole molecule. The rotational potential energy is in principle multidimensional and not separable into the various torsional angles. Two approximative schemes are suitable to reduce the dimensionality of the potential. The easiest way is to keep all variables in their equilibrium values up to one which is the relevant variable in

the reduced one-dimensional rotational potential. The second method is more stringent in the sense that the one-dimensional potential is now determined by some stationary points, corresponding with a full geometry optimization. In this scheme, the $M - 1$ remaining parameters are no longer constant along the path over the rotational barrier, but this approach leads to more realistic values of the rotational barriers.[12] Through the stationary points corresponding with fully optimized stable conformers, one tries to fit a k_{max}-term Fourier expansion

$$V_m(\phi_m) = \sum_{k=1}^{k_{max}} \frac{1}{2} V_{mk}(1 - \cos(k\phi_m)) \tag{6}$$

completely determining the rotational barrier. In our case study, the potential function has high symmetry; hence the series in eq 6 converges very rapidly and only a small number of harmonics are needed. Because we always have more than one harmonic, we cannot use the standard solution procedure available for the case of only one harmonic.[19] Instead, the energy levels of the internal rotations are obtained using an efficient computational algorithm, outlined in the Appendix, which is based on solving the Schrödinger equation on a discretized angular grid. Once the energy levels $\epsilon_k(m)$ are evaluated for each internal rotation m, the partition functions $q_{rot,int}$ can be constructed by the product over the M individual internal rotation partition functions:

$$q_{rot,int,m} = \frac{1}{\sigma_{int}} \sum_k g_k(m) \exp\left(-\frac{\epsilon_k(m)}{k_B T}\right) \tag{7}$$

where $g_k(m)$ is the degeneracy of the rotational energy level $\epsilon_k(m)$ for the mth top and σ_{int} is the symmetry number of the internal rotation.

In this way, one achieves one of the main goals of this reaction study; one has established a microscopic description of the rate constant versus temperature (eq 1). Following the Arrhenius rate law, the reaction rate constant is given by

$$k(T) = Ae^{-E_a/(RT)} \tag{8}$$

where R is the universal gas constant, A is the preexponential factor or frequency factor, and E_a is the activation energy, which are assumed to be temperature independent. On the other hand, in TST the kinetic parameters A and E_a are in principle dependent on T because of their construction (by means of partition functions). We found (section 4.4) that for the reaction under study in the considered temperature range the Arrhenius rate law models the temperature dependence of the rate constant very well. Using eq 1, the rate coefficients at different temperatures are calculated. The two kinetic parameters are then computed by a least-squares fit from a set of rate coefficients at different temperatures determined through eq 1. The results are discussed in section 4.4.

3. Computational Procedures

All calculations were carried out with the Gaussian 98 software package.[20] Furthermore, all calculations were performed within the DFT framework[21] by using Becke's three-parameter hybrid B3LYP functional.[22] The molecular orbitals are expanded in the triple-ζ 6-311G basis augmented with single first d and p polarization functions.[23] Several studies[24−26] have indicated that B3LYP and even HF methods are sufficiently accurate for the estimation of the relative stabilities of different conformers and the calculation of the potential energy profile

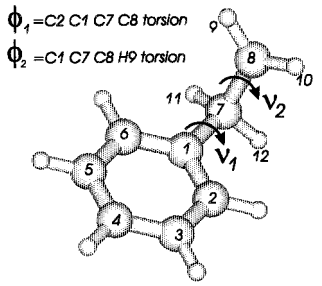

Figure 2. Ground-state configuration of the ethylbenzene radical.

for internal rotation, especially when large basis sets including polarization functions are used. According to specific studies on similar radical reactions,[14] the B3LYP method gives a reliable and quantitatively good description of geometries, frequencies, reaction barriers, and preexponential factors. For this case, in which the system of interest is quite large, B3LYP provides a viable alternative to more computationally intensive methods such as CBS,[27] G2,[28] and CBS-RAD[29] procedures. Energy minima were located by full geometry optimizations with the Berny algorithm.[30,31] The transition structures were located according to the following procedure. At the first stage, all variables but the reaction coordinate are optimized whereas the reaction coordinate was varied stepwise. The maximum of this linear transit served as the starting structure in a transition state optimization using the transit-guided quasi-Newton (STQN) method.[30,31] The vibrational frequencies of the optimized structures and the rotational barriers are also calculated at the same level of theory. It is well-known that the B3LYP harmonic vibrational frequencies are systematically larger than the observed experimental frequencies. The overestimation, however, is found to be relatively uniform, and as a result generic frequency scaling factors are often applied. A scaling factor of 0.9614 is applied to the frequencies in the evaluation of the partition functions,[32] whereas the zero-point vibrational energies are scaled with 0.9806.[32]

In conformation with the general outline given in section 2, the rotational potentials for each of the internal rotations are approximated by one-dimensional functions in the relevant torsional angle. The full rotational potential is then obtained by fitting a three-term Fourier expansion ($k_{max} = 6$ in eq 6) to the energies of the fully optimized stable conformers. The energy eigenvalues for each hindered rotation are evaluated according to the numerical algorithm as outlined in the Appendix. The number of eigenstates chosen is high enough to get sufficient convergence of the rotational partition functions.

4. Results and Discussion

4.1. Reactants. *Geometries.* The reactants for the addition reaction are the ethylbenzene radical and ethene. Figure 2 shows the energetically most favored conformation of the ethylbenzene radical (the EB conformer). The EB conformer has C_s symmetry, with the ethyl chain lying in a plane of symmetry dividing the ring and oriented orthogonally toward it. The radical center is slightly pyramidally displaced because of the asymmetry of the RCH_2 group (the two planes $H_9C_8C_7$ and $H_{10}C_8C_7$ form an angle of 165.6°). Our ab initio calculations reproduce the structure accurately. Because of the presence of the ethyl chain, the D_{6h} symmetry of an isolated benzene ring is partially broken; the two bonds C_6-C_1 and C_2-C_1 near the ethyl chain are somewhat larger (1.398 Å) than the other benzene bonds (1.393 Å). Both values are in close agreement with the experimental estimates of the C−C bond length of benzene (1.397 Å).[33] The ending

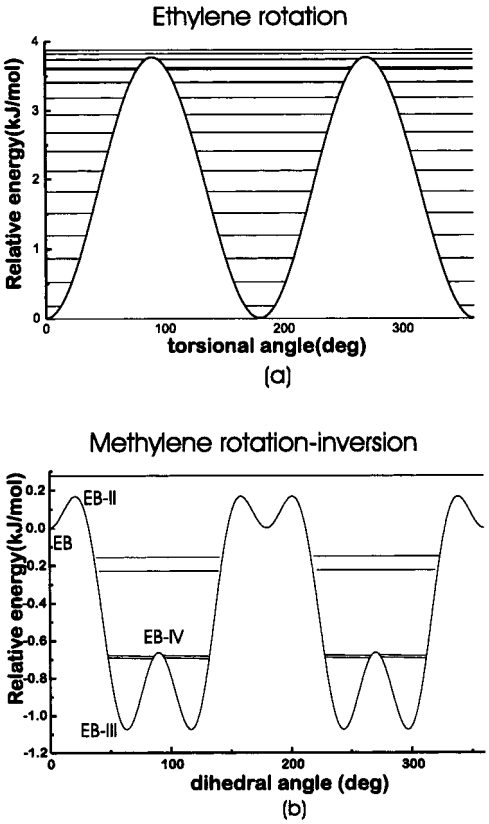

Figure 3. Rotational potentials for the torsional motions in the ethylbenzene radical. The energies are relative with respect to the EB conformer. The torsional angles are relative with respect to the equilibrium geometry of the EB conformer.

C−C bond of the ethyl chain (C_7-C_8 = 1.496 Å) is shorter than experimental estimates of carbon−carbon single bond lengths (propane, 1.541 Å; ethane, 1.538 Å; propene, 1.520 Å[33]) because of the presence of the radical center.

Vibrational Analysis. A vibrational analysis of ethene reveals that the lowest frequency amounts to 833.5 cm^{-1}. Hence, no attention must be paid to internal rotations as could be expected from the rigidity of the π bond in ethene.

Some of the low-frequency modes in the ethylbenzene radical do not correspond with vibrational motions but with internal hindered or unhindered rotations. The lowest vibrational frequencies of the EB conformer lie at $\nu_1 = 39.4$, $\nu_2 = 123.9$, and $\nu_b = 137.9$ cm^{-1}. The vibrational modes ν_1 and ν_2 can be associated with internal rotations belonging to the torsional angles ϕ_1 and ϕ_2, as indicated in Figure 2. The lowest frequency corresponds to a rotation of the ending ethylene (C_2H_4) group around the C_1-C_7 bond, whereas the second represents the rotation of the methylene group CH_2 at the radical terminus. The value of the third frequency is of the same order of magnitude as ν_2 but cannot be associated to an internal rotation. It represents a bending mode of the ethyl chain toward the aromatic ring. This mode will be treated within the harmonic oscillator approximation because of its complexity and the high barriers needed for a significant bending of the important angles.

Torsional Potential Energies. Figure 3a shows the torsional potential for the ethylene rotation in the ethylbenzene radical. The maximum energy conformation corresponds to a geometry in which the ethyl chain has a planar orientation toward the aromatic ring. This structure has C_σ symmetry with a plane of symmetry defined by the aromatic ring and the carbon atoms of the ethyl chain. The reduced moment of inertia for this motion amounts to 85.57 au. In this particular case, the lowest energy

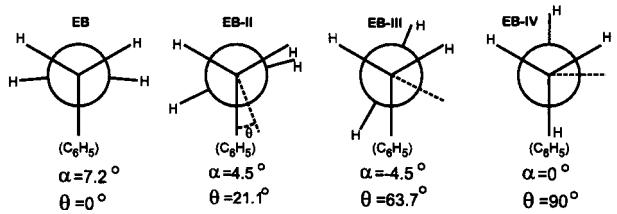

Figure 4. Newman projections of the CH_2 rotation−inversion process in the ethylbenzene radical.

levels found by solving the eigenvalue equation (eq 4) are nearly double-degenerate because of the periodicity of π combined with the high inertial moment of the rotating group ($-\hbar^2/(2I_m)$ = 0.008 kJ/mol) compared with the rotational potential barrier (3.8 kJ/mol). Hence, the degeneracy is nearly canceled by the symmetry number ($\sigma_{int} = 2$) in the evaluation of the partition function. The rotational energy levels are displayed in Figure 3a.

The methylene rotation with a reduced moment of inertia of 6.24 au leads to the rotational potential shown in Figure 3b. It should be noted that the methylene rotation actually corresponds to a rotation−inversion process, a combination of a rotation of the CH_2 group and an inversion at the radical center. This is in complete agreement with the conclusions made in refs 12 and 13. The inversion results in a rotational potential that has six minima with a symmetry number of $\sigma_{int} = 2$. The different stationary points of the CH_2 rotation−inversion process are schematically given in Figure 4. Because of the nonplanarity of the radical carbon center, we need two torsional angles $\phi_2 = C_1C_7C_8H_9$ and $\phi_2' = C_1C_7C_8H_{10}$ in order to determine unambiguously the combined rotation and inversion process. However, the mechanism of the process is better described by introducing two new parameters α and θ related to ϕ_2 and ϕ_2' by

$$\alpha = 90° - (\phi_2' - \phi_2)/2$$

$$\theta = (\phi_2' + \phi_2)/2$$

α is a measure of nonplanarity (see Figure 4), and θ is the dihedral angle. We notice that the potential associated with the rotation−inversion process, as shown in Figure 3b, is plotted versus the dihedral angle θ instead of the torsional angle ϕ_2, respecting in this way the periodicity π. The results of the Fourier fitting procedure are listed in Table 1.

4.2. Products. *Geometries.* The product of the addition reaction is the butylbenzene radical. Also, for this radical different conformers exist, distinguished from each other by internal rotations. To locate different stationary points on the potential energy surface, we performed a full conformational analysis of the butylbenzene radical. A conformational analysis on *n*-butylbenzene has been done by Dickinson et al.[34] Five stable minima were located on the potential energy surface. For each, the angle between the butyl chain and the benzene plane is approximately 90° and the combination of gauche and anti orientations of the remaining CCCC torsions in the butyl chain generates five stable conformers. We found a strong conformational analogy between *n*-butylbenzene and its primary radical, but because of the H-abstraction and the resulting sp^2 hybridization, one would expect the methylene torsional potential (ϕ_4) to have six minima instead of three. This would double the five unique minima of butylbenzene in its H-abstracted radical. However, a conformational analysis reveals that only two conformers (BB1 and BB2, see Figure 6) generate six minima for the methylene rotation−inversion whereas large

TABLE 1: Geometrical Parameters and Rotational Potentials for the Different Internal Rotations in the Ethylbenzene Radical[a]

	ab initio calculations		Fourier fit results		
ethylene rotation	ϕ_1	E_0^{rel}	I_m	V_i	ϕ_1^f
EB	0.0	0.0	85.57	$V_2 = 3.771$	0.0
	89.2	3.770			89.2

methylene rotation−inversion	ab initio calculations		Fourier fit results		
	θ	E_0^{rel}	I_m	V_i	θ^f
EB	0.0	0.0	6.24	$V_2 = -1.188$	0.0
EB-II	21.1	0.167		$V_4 = -0.218$	22.5
EB-III	63.7	−1.074		$V_6 = 0.526$	70.5
EB-IV	90.0	−0.662			90.0

[a] E_0^{rel} is the relative energy (kJ/mol) with respect to the ground-state energy of the EB conformer (−310.286 554 au) with the exclusion of ZPE. V_i is expressed in kJ/mol. The angles are relative to the equilibrium values of the EB conformer: $\phi_1 = -89.2°$ and $\phi_2 = -82.8°$. ϕ_1^f and θ^f are the angles as obtained from the Fourier fitting procedure. I_m is the reduced moment of inertia (au) for each individual rotation.

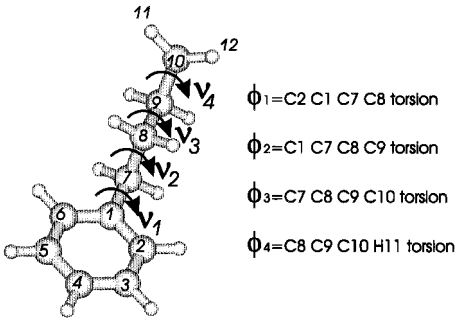

Figure 5. Definition of torsional angles in the butyl chain.

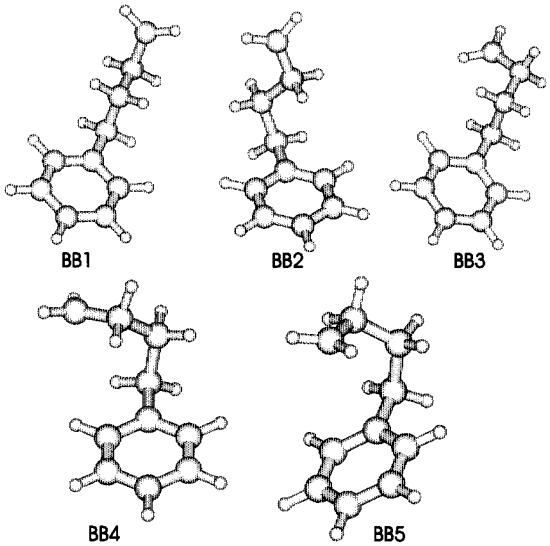

Figure 6. Stable conformers of the butylbenzene radical. BB1′ and BB2′ are not taken up, because they differ only in the methylene rotation.

steric hindrance in the other conformations prevents the appearance of additional minima. We define the torsional angles ϕ_1, ϕ_2, ϕ_3, and ϕ_4 as indicated in Figure 5. The geometrical values for the torsional angles are listed in Table 2 as well as total binding energies relative to the BB1 conformer. In Figure 6, we display the five main local minima for the primary radical. We do not take up BB1′ and BB2′ as they differ only in the methylene torsional angle ϕ_4. BB1 and BB3 are both anti conformers for the orientation of the side chain about the C_7-C_8 bond. Both stable structures are further distinguished by their orientations about the C_8-C_9 bond. BB2, BB4, and BB5 are gauche conformers about the C_7-C_8 bond and are further split up by anti and two possible staggered orientations of the radical terminus around the C_8-C_9 bond.

TABLE 2: Geometrical Parameters for the Stable Conformers of the Butylbenzene Radical[a]

	ϕ_1	ϕ_2	ϕ_3	ϕ_4	E_0^{rel}
BB1	−89.130	180.0	180.0	−85.330	0.0
BB2	−73.503	−65.615	179.0	−35.1	1.86
BB3	−87.2	179.1	−66.7	150.2	0.27
BB4	−101.3	65.2	64.8	−155.2	1.96
BB5	−70.7	−71.5	70.8	−143.1	8.03
BB1′	−88.3	−179.8	178.5	−33.0	−0.206
BB2′	−75.1	−65.4	−177.5	32.0	1.97

[a] ϕ_1, ϕ_2, ϕ_3, and ϕ_4 are the torsional angles as defined in Figure 5. E_0^{rel} is the total binding energy (kJ/mol) relative to the BB1 conformer (−388.935 91 au) with the exclusion of ZPE.

TABLE 3: Lowest Vibrational Frequencies (in cm^{-1}) for Different Conformers of the Butylbenzene Radical

	BB1	BB2	BB3	BB4	BB5
ν_1	21.2	35.7	34.8	29.0	92.3
ν_2	118.3	119.8	50.5	50.8	86.7
ν_3	88.1	64.9	143.8	168.6	142.9
ν_4	54.9	77.2	127.6	137.3	252.0
ν_{sk}	80.1	167.8	95.7	105.5	183.2

The lowest energy conformer of the butylbenzene radical (BB1, apart from BB1′) has a similar structure to the EB conformer and is chosen as the reference conformer because of its higher symmetry compared with BB1′. The BB1 conformer exhibits a C_s symmetry with the butyl chain oriented orthogonally toward the aromatic ring. The bond lengths of the carbon atoms forming the ring are very similar to those in the ethylbenzene radical; the two C−C bonds near the butyl chain (1.399 Å) are larger than the four other bonds (1.393 Å). The C−C bond connected to the radical center (1.489 Å) shows the same trends as observed in the EB conformer. For the other C−C bonds of the alkyl chain ($C_7-C_8 = 1.541$ and $C_8-C_9 = 1.550$ Å), excellent agreement with experiment is reached (propane, 1.541; ethane, 1.538; propene, 1.520; isobutane, 1.545 Å[33]).

Vibrational Analysis. The identification of the internal rotations in the butylbenzene radical requires a vibrational analysis of all structures. Table 3 lists the lowest vibrational frequencies for all stable conformers. The vibrations of the BB1 conformer are examined in more detail. ν_1, ν_2, ν_3, and ν_4 represent internal rotations associated with variations of the torsional angles ϕ_1, ϕ_2, ϕ_3, and ϕ_4 as indicated in Figure 5. ν_1 corresponds to a rotation of the butyl chain around the C_1-C_7 bond, and ν_2 can be associated with the rotation of the side chain around the C_7-C_8 bond. ν_3 corresponds with a rotation of the ethylene (CH_2-CH_2) around the C_8-C_9 bond, and finally ν_4 represents the methylene (CH_2) rotation at the radical terminus. ν_{sk} is a low-lying frequency associated with a skeletal vibration. These vibrations arise in larger structures, and their frequencies are of the same order of magnitude as those of internal rotations. The higher the mass of the cluster involved in the skeletal motion, the lower the corresponding frequency ν_{sk}. These skeletal vibrations are treated within the harmonic oscillator approximation. Because they are present in products, reactants, and transition states, their global contribution to the equilibrium constant $K_C^{\ddagger}$ is small as a result of canceling of their relevant fractions in the partition functions. In this paper, the motions corresponding to ν_1, ν_2, ν_3, and ν_4 frequencies will be referred

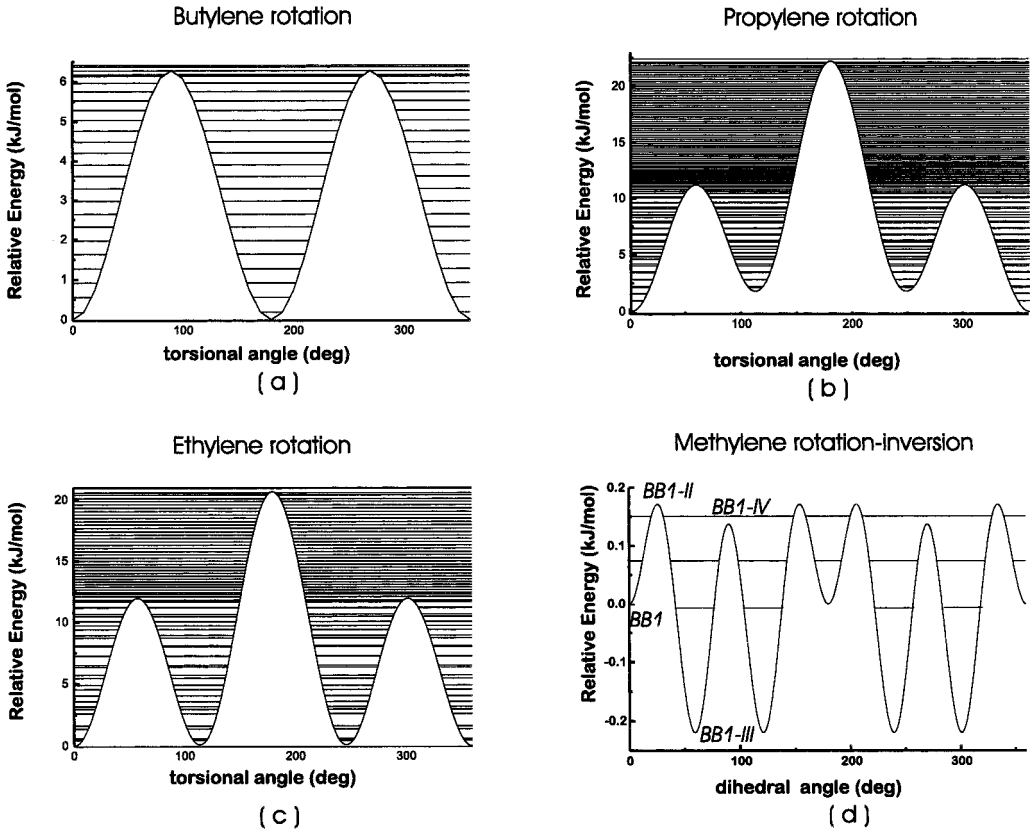

Figure 7. Rotational potentials for the torsional motions in the butylbenzene radical. The energies are relative with respect to the BB1 conformer. The torsional angles are relative with respect to the equilibrium geometry of the BB1 conformer.

to as butylene, propylene, ethylene, and methylene rotations, respectively. For the six other stable conformers (BB2, BB3, BB4, BB5, BB1′, and BB2′), we notice the same pattern of low vibrational motions but the frequencies can vary significantly when going from one conformation to another. This is best illustrated for the mode corresponding to the rotation of the methylene group around the C_9-C_{10} bond; the frequency for this mode increases from 54.9 to 252.0 cm^{-1} in going from the BB1 to the BB5 conformer. This can be understood as follows; in the BB1 conformer, the rotation of the ending methylene group is nearly free, whereas in the BB5 conformer this internal motion is much more hindered because of the presence of the benzene ring in the near vicinity of the methylene group.

Torsional Potential Energies. The rotational potentials associated with the internal rotations are determined by following the procedure explained in section 2. We make use of the fully optimized conformers of the butylbenzene radical. Also, the energy maxima in terms of the different torsional angles are determined by complete geometry optimizations. Figure 7 shows the rotational potentials for the four internal rotations of the butylbenzene radical, and Table 4 lists the results of the Fourier fitting procedure and the reduced moments of inertia.

The butylene rotation has two stationary points in a period of π corresponding to an orthogonal and planar orientation of the butyl chain toward the ring. For the propylene and ethylene rotations, the potential energy profile is very similar to the well-known CCCC rotational profile found in *n*-butane. The minima correspond to anti and gauche orientations of the rotating groups, whereas the maxima are associated with eclipsed conformations. Both motions are schematically depicted in Figure 8. The rotational potential for the methylene rotation, starting from the BB1 conformer, is similar to the one found in the ethylbenzene radical, although the rotational barriers are lower in the BB1 conformer and differences in the relative heights of the maxima are noticed. In the ethylbenzene radical, the methylene rotation is more hindered because of the aromatic ring, leading to higher rotational barriers. The pyramidalization is reduced in the BB1 conformer ($H_{11}C_{10}H_{12}C_9$ dihedral angle = 171.6°), leading to a shift of the relative maxima. Newman projections for the methylene rotations are shown in Figure 8.

4.3. Transition States. *Geometries.* From the conformational analysis of the butylbenzene radical, we can expect the existence of five transition states which are interconverted into each other by internal rotations. To locate the transition structures, we followed the procedure outlined in section 3, in which the reaction coordinate was approximated by the decreasing C−C distance of the forming bond. Table 5 shows several key geometrical parameters for the different transition structures which are referred to as TSBB1, TSBB2, TSBB3, TSBB4, and TSBB5. The forming C−C bond reaches approximately 2.3 Å in all structures. Figure 9 shows the structures of the different conformers.

Vibrational Analysis. A detailed vibrational analysis for all optimized transition states is performed. When two nonlinear molecules, each having $3N_i - 6$ vibrational degrees of freedom (N_i is the number of atoms in molecule i), are brought together to form one global molecule, six additional vibrational modes appear in the product state and in the transition state. These modes are called *transitional modes* and arise from the loss of translational and external rotational motions of the approaching species. One of the newly formed modes has an imaginary frequency in the transition state and can be associated with a translational or loose vibrational motion along the reaction coordinate. For the conformer TSBB1, the lowest real vibrational frequencies are located at $\nu_1 = 67.94$, $\nu_2 = 39.91$, $\nu_3 = 28.26$, and $\nu_{sk} = 63.04$ cm^{-1}. The vibrational frequencies ν_1, ν_2, and

TABLE 4: Geometrical Parameters and Rotational Potentials for the Different Internal Rotations in the Butylbenzene Radical[a]

	ab initio calculations		Fourier fit results		
butylene rotation	ϕ_1	E_0^{rel}	I_m	V_i	ϕ_1^f
BB1	0.0	0.0	128.01	$V_2 = 6.275$	0.0
	90.0	6.28			90.0

	ab initio calculations		Fourier fit results		
propylene rotation	ϕ_2	E_0^{rel}	I_m	V_i	ϕ_2^f
BB1	0.0	0.0	178.30	$V_1 = 8.935$	0.0
TSBB1-BB2	60.2	11.20		$V_2 = -5.738$	61.5
BB2	114.8	1.86		$V_3 = 13.272$	113.9
TSBB2-BB2	180.0	22.21			180.0

	ab initio calculations		Fourier fit results		
ethylene rotation	ϕ_3	E_0^{rel}	I_m	V_i	ϕ_3^f
BB1	0.0	0.0	93.007	$V_1 = 6.164$	0.0
TSBB1-BB3	58.743	11.97		$V_2 = -5.491$	60.3
BB3	110.0	0.27		$V_3 = 14.516$	115.6
TSBB3-BB3	180.0	20.68			180.0

	ab initio calculations		Fourier fit results		
methylene rotation−inversion	θ	E_0^{rel}	I_m	V_i	θ^f
BB1	0.0	0.0	6.179	$V_2 = -0.159$	0.0
BB1-II	28.01	0.179		$V_4 = -0.132$	27.2
BB1-III (BB1′)	61.25	−0.206		$V_6 = 0.297$	60.2
BB1-IV	90.0	0.146			90.0

[a] E_0^{rel} is the relative energy (kJ/mol) with respect to the ground-state energy of the BB1 conformer (−388.935 91 au) with the exclusion of ZPE. V_i is expressed in kJ/mol. The angles are relative to the equilibrium values of the BB1 conformer: $\phi_1 = -89.1°$, $\phi_2 = 180.0°$, $\phi_3 = 180.0°$, and $\phi_4 = -85.330°$. ϕ_1^f, ϕ_2^f, ϕ_3^f, and θ^f are the angles as obtained from the Fourier fitting procedure. I_m is the reduced moment of inertia (au) for each individual rotation.

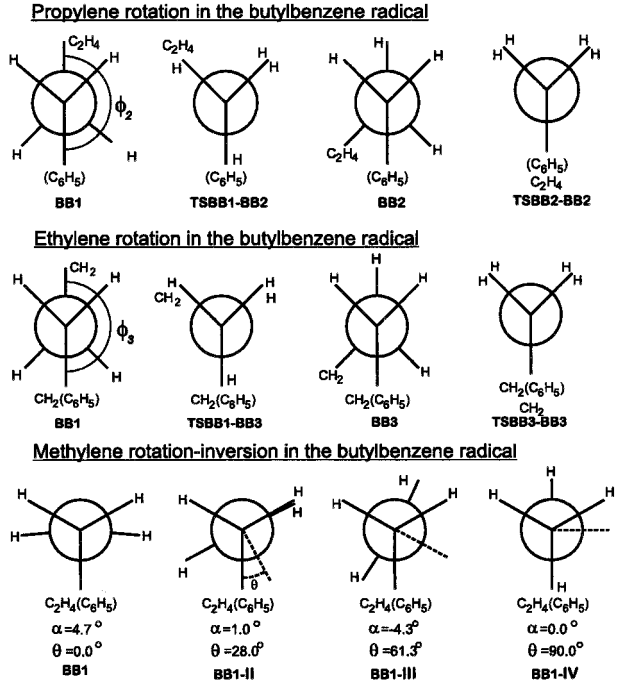

Figure 8. Newman projections of the internal rotations in the butylbenzene radical.

ν_3 correspond with the torsional angles ϕ_1, ϕ_2, and ϕ_3, respectively (Figure 9). The lowest real frequency ν_3 corresponds to an internal rotation of the approaching ethene about the forming C−C bond. This mode arises from the loss of one external rotation of ethene when brought together with the ethylbenzene radical in the transition state. This motion is one of the transitional modes. The second lowest frequency ν_2 corresponds with a rotation of both the approaching ethene and the CH_2 at the radical terminus around the C_7-C_8 bond (this rotation will be referred to as the propylene rotation). This kind of motion was also present in the ethylbenzene radical as an internal rotation of the methylene group and thus cannot be identified as a transitional mode. ν_{sk} is characterized as a bending mode of the two approaching species in the transition state. It can clearly be identified as one of the transitional modes because it arises from the loss of translational and rotational motions of the separate molecules in the reactants. ν_1 corresponds to an internal rotation of the forming butyl chain about the C_1-C_7 bond. Because an analogous motion was also present in the ethylbenzene radical, we cannot identify it as one of the transitional modes. Further inspection of the vibrational modes enables us to characterize the other three real transitional modes. They are all low-lying frequencies (below 1000 cm^{-1}), but they do not correspond with pure rotational motions. Because of their complexity, we will treat them in the harmonic oscillator approximation. In summary, the transition state exhibits three relevant internal rotations. The rigidity of the double bond of ethene prevents the methylene rotation. The torsional motions belonging to the internal rotations are schematically depicted in Figure 9.

TABLE 5: Geometrical Values for the Five Transition Structures[a]

	C−C (Å)	ϕ_1	ϕ_2	ϕ_3	ϕ_4	E_0^{rel}
TSBB1	2.313	−89.1	180.0	180.0	−87.9	0.0
TSBB2	2.303	−71.1	−73.0	180.0	−88.2	3.335
TSBB3	2.311	−90.1	177.9	−53.5	87.5	−1.286
TSBB4	2.300	−107.8	71.8	57.5	86.8	−0.84
TSBB5	2.300	−68.7	−68.1	88.8	88.1	5.33

[a] ϕ_1, ϕ_2, ϕ_3, and ϕ_4 are the torsional angles as defined in Figure 5. E_0^{rel} is the total binding energy (kJ/mol) relative to the TSBB1 transition state conformer ($E_0 = -388.891\,130$ au).

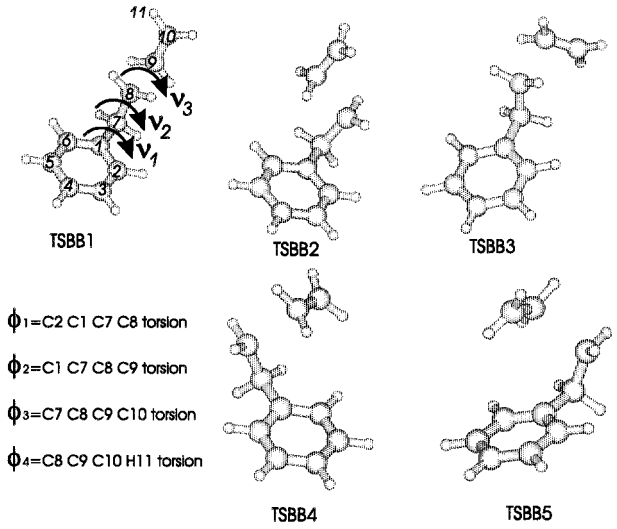

Figure 9. Structures of the different transition states.

Torsional Potential Energies. We apply similar procedures as in section 4.2 for the evaluation of the rotational potentials for the three internal rotations present in the transition state. They are displayed in Figure 10, and the relevant numerical parameters are listed in Table 6. The rotational potentials for the butylene and propylene rotations are very similar to their behavior in the BB1 conformer. For the ethylene rotation, a

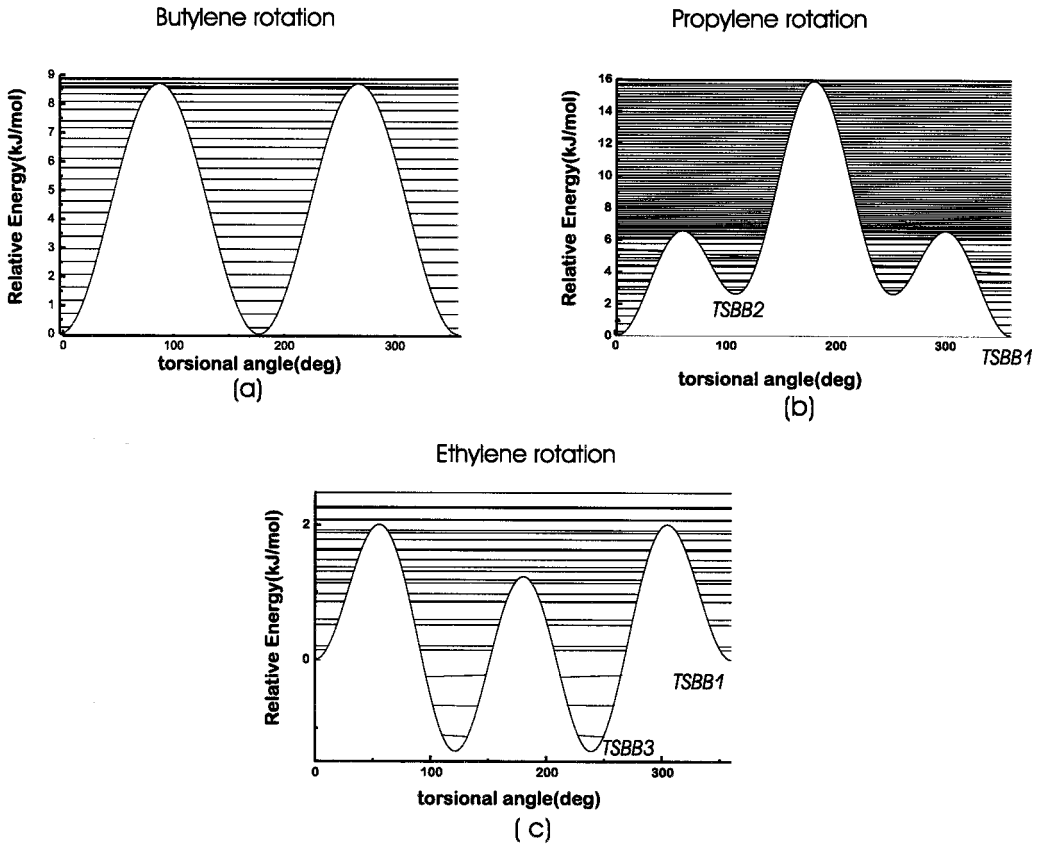

Figure 10. Rotational potentials for the torsional motions in the transition state for the anti addition. The energies are relative with respect to the TSBB1 conformer. The torsional angles are relative with respect to the equilibrium geometry of the TSBB1 conformer.

TABLE 6: Geometrical Parameters and Rotational Potentials for the Different Internal Rotations in the Transition State[a]

	ab initio calculations		Fourier fit results		
butylene rotation	ϕ_1	E_0^{rel}	I_m	V_i	ϕ_1^f
TSBB1	0.0	0.0	109.603	$V_2 = 8.708$	0.0
	90.0	8.71			90.0

	ab initio calculations		Fourier fit results		
propylene rotation	ϕ_2	E_0^{rel}	I_m	V_i	ϕ_2^f
BB1	0.0	0.0	265.48	$V_1 = 8.437$	0.0
TSBB1-TSBB2	60.0	6.56		$V_2 = -3.990$	60.0
TSBB2	120.0	3.34		$V_3 = 7.448$	120.0
TSBB2-TSBB1	180.0	15.89			180.0

	ab initio calculations		Fourier fit results		
ethylene rotation	ϕ_3	E_0^{rel}	I_m	V_i	ϕ_3^f
TSBB1	0.0	0.0	84.60	$V_1 = -1.384$	0.0
TSBB1-TSBB3	60.0	1.97		$V_2 = -0.399$	56.3
TSBB3	126.5	−1.29		$V_3 = 2.614$	122.0
TSBB3-TSBB1	180.0	1.23			180.0

[a] E_0^{rel} is the relative energy (kJ/mol) with respect to the energy of the TSBB1 conformer (−388.891 130 au) with the exclusion of ZPE. V_i is expressed in kJ/mol. The angles are relative to the equilibrium values of the TSBB1 conformer: $\phi_1 = -89.1°$, $\phi_2 = 180.0°$, and $\phi_3 = 180.0°$. ϕ_1^f, ϕ_2^f, and ϕ_3^f are the angles as obtained from the Fourier fitting procedure. I_m is the reduced moment of inertia (au) for each individual rotation.

structural change of the rotational potential is noticed when going from the transition state to the butylbenzene radical. This could be expected because the ethylene rotation is one of the transitional modes. From Figure 10c, it follows that a gauche attack of the ethylbenzene radical is energetically favored over an anti attack. This result was also found by Heuts et al.[12] for a similar radical addition reaction, namely, the addition of the ethyl radical to ethene.

4.4. Activation Barriers and Rate Constants for the Forward and Reverse Reaction. On the basis of the performed theoretical ab initio calculations, we are able to obtain a reliable prediction for empirical parameters such as the preexponential factor A and the activation energy E_a. In transition state theory, the ab initio microscopic results are related to macroscopic kinetic properties A and E_a by the rate equation (eq 1), which requires the evaluation of the molecular partition functions of the reactants, products, and transition state. They are tabulated in Table 7 for temperatures ranging from 100 to 1000 K. The full partition functions unambiguously determine the equilibrium constants, which allows us to construct an Arrhenius plot for the forward and reverse reaction, as displayed in Figure 11. A and E_a may now be determined by fitting a linear function to the data points by means of a least-squares method. The slope of this best-fit line gives the activation energy, and the intercept leads to the preexponential factor. The results are listed in Table 8. ZPE is the zero-point vibrational energy scaled with 0.9806 according to ref 32. The units of the rate constant and consequently the preexponential factor depend on the stoichiometry of the chemical reaction. The forward reaction is of second order, and therefore A has units of $dm^3\ mol^{-1}\ s^{-1}$. The reverse reaction is of first order with units of s^{-1} for the rate constant.

Figure 11 clearly shows that for the reaction under consideration the Arrhenius rate law represents the temperature dependence of the rate constant very well. The activation energy is largely determined by the molecular energy difference at absolute zero between the activated complex and the reactants, but the implementation of internal rotations may cause a non-

TABLE 7: Partition Functions and Equilibrium Constants for the Forward and Reverse Reactions[a]

T	q_{EB}	q_{eth}	q_{BB1}	q_{TSBB1}	$K_C^{\ddagger forward}$	$K_C^{\ddagger reverse}$
All Vibrations Treated within Harmonic Oscillator Approximation						
100	1.11×10^{12}	4.79×10^{7}	2.96×10^{13}	3.51×10^{13}	4.11×10^{-23}	8.39×10^{-59}
200	9.20×10^{13}	7.71×10^{8}	1.08×10^{16}	1.25×10^{16}	1.39×10^{-15}	9.71×10^{-30}
300	2.68×10^{15}	4.11×10^{9}	1.01×10^{18}	1.14×10^{18}	4.10×10^{-13}	4.65×10^{-20}
400	5.59×10^{16}	1.48×10^{10}	5.94×10^{19}	6.59×10^{19}	7.10×10^{-12}	3.22×10^{-15}
500	9.90×10^{17}	4.39×10^{10}	2.78×10^{21}	3.05×10^{21}	4.03×10^{-11}	2.57×10^{-12}
600	1.56×10^{19}	1.17×10^{11}	1.11×10^{23}	1.20×10^{23}	1.32×10^{-10}	2.20×10^{-10}
700	2.20×10^{20}	2.88×10^{11}	3.48×10^{24}	4.09×10^{24}	3.12×10^{-10}	5.24×10^{-9}
800	2.80×10^{21}	6.71×10^{11}	1.16×10^{26}	1.21×10^{26}	6.06×10^{-10}	5.61×10^{-8}
900	3.23×10^{22}	1.49×10^{12}	3.08×10^{27}	3.13×10^{27}	1.03×10^{-9}	3.51×10^{-7}
1000	3.38×10^{23}	3.18×10^{12}	7.23×10^{28}	7.13×10^{28}	1.59×10^{-9}	1.51×10^{-6}
Internal Rotations Explicitly Treated						
100	4.41×10^{12}	4.79×10^{7}	4.08×10^{13}	2.10×10^{14}	5.07×10^{-23}	1.27×10^{-58}
200	3.12×10^{14}	7.71×10^{8}	3.98×10^{16}	8.83×10^{16}	2.63×10^{-15}	1.10×10^{-29}
300	8.01×10^{15}	4.11×10^{9}	5.38×10^{18}	9.62×10^{18}	1.08×10^{-12}	5.20×10^{-20}
400	1.48×10^{17}	1.48×10^{10}	3.78×10^{20}	6.10×10^{20}	2.36×10^{-11}	3.60×10^{-15}
500	2.34×10^{18}	4.39×10^{10}	1.93×10^{22}	2.93×10^{22}	1.57×10^{-10}	2.87×10^{-12}
600	3.31×10^{19}	1.17×10^{11}	8.03×10^{23}	1.15×10^{24}	5.75×10^{-10}	2.45×10^{-10}
700	4.24×10^{20}	2.88×10^{11}	2.80×10^{25}	3.84×10^{25}	1.48×10^{-9}	5.82×10^{-9}
800	4.93×10^{21}	6.71×10^{11}	8.37×10^{26}	1.10×10^{27}	3.06×10^{-9}	6.21×10^{-8}
900	5.23×10^{22}	1.49×10^{12}	2.17×10^{28}	2.74×10^{28}	5.43×10^{-9}	3.89×10^{-7}
1000	5.07×10^{23}	3.18×10^{12}	4.90×10^{29}	5.97×10^{29}	8.68×10^{-9}	1.68×10^{-6}

[a] T is the temperature expressed in K. q_{EB}, q_{eth}, q_{BB1}, and q_{TSBB1} are the molecular partition functions of the ethylbenzene radical, ethene, the butylbenzene radical, and the transition state, respectively. $K_C^{\ddagger forward}$ and $K_C^{\ddagger reverse}$ are the equilibrium constants associated with the forward and reverse anti addition reactions.

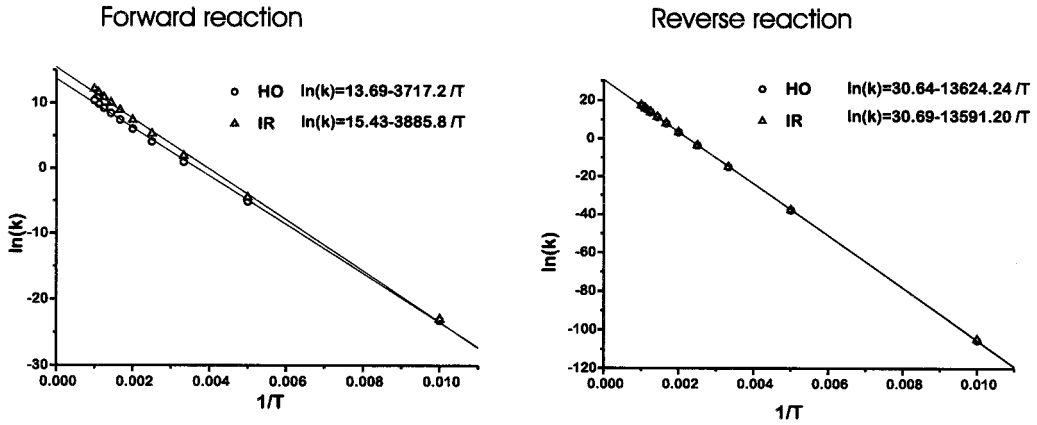

Figure 11. Arrhenius plot of ln k versus $1/T$ for the forward reaction and reverse reaction.

TABLE 8: Energies and Kinetic Characteristics for the Anti Addition Reaction[a]

	C_2H_2	$C_6H_5C_2H_4^{\bullet}$	$[C_6H_5C_2H_4 - C_2H_2^{\bullet}]^{\ddagger}$	$C_6H_5C_4H_8^{\bullet}$
E_0 (au)	−78.613 978	−310.286 554	−388.891 130	−388.935 907
ZPE (au)	0.049 831	0.138 612	0.190 857	0.193 232

	$C_6H_5C_2H_4^{\bullet} + C_2H_2 \rightarrow C_6H_5C_4H_8^{\bullet}$	$C_6H_5C_4H_8^{\bullet} \rightarrow C_6H_5C_2H_4^{\bullet} + C_2H_2$
ΔE_0 (kJ/mol)	31.02	111.33
$\Delta E_0'$ (kJ/mol)	31.19	112.21
E_a^{HO} (kJ/mol)	30.91	113.28
A^{HO}	8.8×10^{5}	2.0×10^{13}
E_a^{IR} (kJ/mol)	32.31	113.0
A^{IR}	5.0×10^{6}	2.1×10^{13}

[a] E_0 is the total binding energy of the ground-state configuration. Zero-point vibration energies (ZPE) scaled with 0.9806.[32] ΔE_0 is the molecular energy difference (ab initio DFT) between the transition state and the reactants with the inclusion of ZPE. $\Delta E_0'$ represents ΔE_0 with subtraction of the ZPE of those vibrations which stand for internal rotations. E_a^{HO} and A^{HO} are the activation energy and the preexponential factor calculated with all vibrational motions treated within the harmonic oscillator approximation, whereas E_a^{IR} and A^{IR} are equivalent quantities calculated with explicit consideration of internal rotations and corrected for the corresponding ZPE. A is expressed in units of $dm^3\ mol^{-1}\ s^{-1}$ for the forward reaction and s^{-1} for the reverse reaction.

negligible shift of E_a, which amounts to 1.4 kJ/mol in the forward reaction. This shift can be attributed to two processes:

(1) The choice of the reference conformers, which do not always coincide with the energetically most favored minima, as clearly seen from the conformational study of the internal rotations. In the forward reaction, this effect accounts for only −0.21 kJ/mol, making the activation energy even lower.

(2) The level density of the eigenstates of the internal rotational potentials determining the partition functions. In the forward reaction, the pure internal rotational partition functions

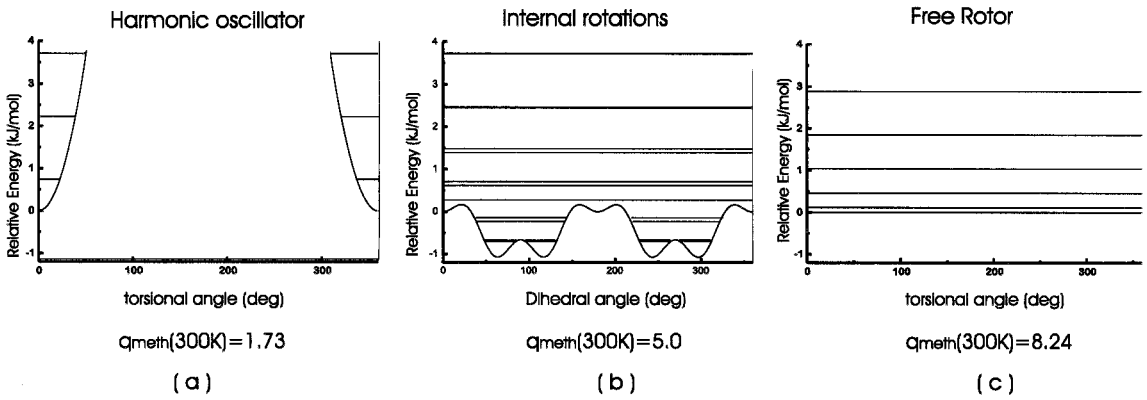

Figure 12. Energy spectrum for the methylene rotation in the EB conformer in the (a) harmonic oscillator, (b) internal rotation, and (c) free rotor (with fixed axis) approximations.

are responsible for an enhancement of 1.3 kJ/mol versus −0.3 kJ/mol in the case of the harmonic oscillator.

The shift of the activation energy in the reverse reaction turns out to be very small. This is due to a cancellation of the two effects mentioned above.

The impact of internal rotations on the preexponential factor is very large. This effect is most striking in the forward reaction, because the partition functions vary most strongly when going from the reactants, consisting of two separate molecules with a large amount of spatial freedom, to the activated complex, in which new, stiffer vibrational modes are formed. When going in the reverse direction from the butylbenzene radical to the activated complex, this change is almost negligible because the geometries and spatial motions are very much alike for both structures.

The preexponential factors are almost completely determined by the vibrational and rotational partition functions. Internal rotations may largely increase the partition functions of the reactants, products, and activated complex. One can question which mechanism underlies this increment. The partition functions of vibrational motions and hindered rotations are largely affected by the density of states in the low-energy spectrum. A study of the methylene rotation in the ethylbenzene radical (Figure 12) shows that the partition functions may be subjected to large variations depending on the method of constructing the energy levels. When treated as a vibrational mode in the harmonic oscillator approximation, the energy levels are equidistant and the interlevel energy spacing is determined by the force constant k of the harmonic oscillator potential at the equilibrium value of the torsional angle ϕ_2. We found a value of $k = 9.5$ kJ/mol in this specific case, and the results are displayed in Figure 12a. In the other limiting case, the methylene rotation is treated as a free rotor about a fixed axis. The energy levels $\epsilon_n = [\hbar^2/(2I_m)]n^2$, where n is an integer, exhibit a 2-fold degeneracy (except for the $n = 0$ ground state) (see Figure 12c). When treating the internal rotations on an exact quantum mechanical basis, we notice an increase of the level density (Figure 12b) compared with the pure harmonic oscillator case. The partition function lies between the two limiting values. The harmonic oscillator approach restricts the methylene group to only small amplitude vibrations. This is not a realistic picture; the small rotational barriers are easily crossed through thermal agitation. This effect amounts to an increase of the partition function by a factor of 3.

Another relevant case study concerns the ethylene and propylene rotations in the TSBB1 conformer of the transition state (Figure 13). The high inertial moments of the rotating groups ($\hbar^2/(2I_m) = 0.009$ and 0.0027 kJ/mol for ethylene and

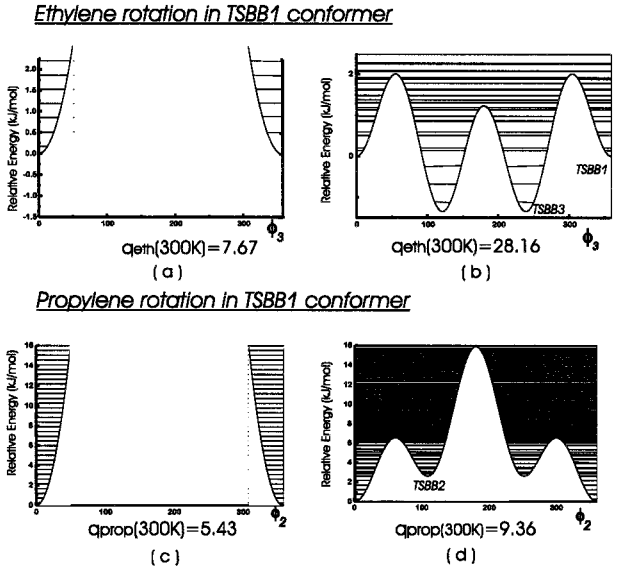

Figure 13. Energy spectrum for some torsional motions in the TSBB1 conformer in the harmonic oscillator and internal rotation approximations.

propylene, respectively) compared with the corresponding rotational potential barriers which are 3 orders of magnitude larger make a comparative study with the free rotor case senseless. Once more, the handling of rotations as small amplitude vibrations prevents the molecule from occupying rotational levels over the whole rotational range between ϕ_2 and ϕ_3. The two one-dimensional rotations over ϕ_2 and ϕ_3 make other stable conformers such as TSBB2 and TSBB3 directly reachable from TSBB1, as easily seen in Figure 10b,c. This last conformer has been regarded as the reference conformer in order to respect the consistency with the anti conformation which is most stable in the product. The two remaining conformers, TSBB4 and TSBB5, are populated only by two-step processes (a successive variation of the two torsional angles). The potential barriers to reach them are not correctly described in this decoupled picture. Nevertheless, the global effect of the one-dimensional rotations on the partition functions is large. For the ethylene rotation in the transition state, the presence of two stable conformers, which are almost equally populated statistically, enlarges the partition function by a factor of 4. This specific rotation is mainly responsible for the serious enhancement of the equilibrium constant in the preexponential factor of the forward reaction (see Table 8).

Because no experimental data are available for the reaction under consideration, a direct comparative study of calculated

and experimental values for A and E_a is impossible. Therefore, we compare the theoretical predictions with similar radical addition reactions. A vast amount of experimental data can be found in the literature concerning free-radical polymerization of ethene. For the addition of the ethyl radical to ethene, experimental values for E_a are reported that vary between 27.2 and 36.0 kJ/mol for the forward reaction[35] and between 116.4 and 121.8 kJ/mol for the reverse reaction,[36] depending on the experimental technique used, temperature, and pressure conditions. For the preexponential factor, the values range from 1×10^8 to 1×10^{11} dm^3 mol^{-1} s^{-1} and from 5×10^{12} to 4×10^{13} s^{-1} for the forward and backward reactions, respectively.

Our predictions for the activation energy are of the same order of magnitude as the experimental values for similar addition reactions. In the preceding discussion, we stressed the importance of internal rotations to the preexponential factor A. We found that they lie at the origin of a drastic enhancement of A for the forward reaction, bringing its value closer to the experimental estimate. However, the theoretical value is still 2 orders of magnitude smaller. This discrepancy can be attributed to two factors:

(1) The experimental value does not correspond to the same reaction but to the addition of the ethyl radical to ethene. Because of the presence of the aromatic ring in the ethylbenzene radical, the overall rigidity of the species undergoing reaction is increased and the relative importance of external rotations and translations is reduced as compared with smaller species such as the ethyl radical. This effect was also found by Heuts et al.[13] for the free-radical polymerization of ethene; they also found a decrease of the frequency factor by replacing the ethyl radical by larger macroradicals.

(2) We restricted our calculations to one-dimensional internal rotations about a fixed axis. Some stable conformers are reachable only by a path through a two-dimensional rotational potential surface. An exact treatment of this type of coupled internal rotation requires a suitable algorithm to solve a two-dimensional Schrödinger equation with cross terms in the kinetic energy contributions and with a rotational potential depending on the two torsional angles. This work is in progress. One might expect that these coupled internal rotations will further increase the relevant partition function and hence the preexponential factor for the forward reaction.

We can make the same observations regarding the frequency factor of the reverse reaction.

5. Conclusions

One of the main reactions from the coke formation network, the addition of a primary ethylbenzene radical to ethene, has been studied in detail in order to predict ab initio theoretical values for experimentally relevant kinetic parameters. This study has been performed within the framework of transition state theory. All ab initio calculations have been performed at the DFT-B3LYP level of theory. This method is known to give reliable predictions of geometries, frequencies, and energies for radical reactions.[14,24] First, all stable conformers of the reactants, products, and transition states have been determined by full geometry optimizations. This conformational investigation was followed by a detailed analysis of all vibrational modes that take place in all species under study. Some vibrational modes corresponding to low frequencies are identified as internal rotations. All internal rotations in one torsional angle have been investigated in detail. The various rotational potentials have been constructed by locating all energy maxima connecting the stable conformers. The rotational eigenvalue problems were solved in an exact way. The obtained energy eigenvalues serve as input for the evaluation of the microscopic molecular partition functions at different temperatures (100−1000 K). Once the molecular partition functions are determined, one is able to deduce the rate constant of the reaction under study by means of transition state theory. The temperature dependence of the reaction under study is adequately described by the Arrhenius rate law, yielding theoretical predictions for the activation energy and preexponential factor. The influence of internal rotations on the above kinetic parameters has been studied in detail. These rotations may alter the activation energy within 1.4 kJ/mol, and they enlarge in a substantial way the preexponential factor of the forward reaction, bringing the theoretical prediction closer to the experimental estimate. This feature is not surprising because in the "internal rotation" approach, the number of states in which the molecule can reside due to thermal agitation is much larger compared with the harmonic oscillator approximation. Here, thermal agitation of the molecule is restricted to small amplitude motions, and the infinite oscillator potential hinders the feeding of other stable configurations as well in the reactants, products, and activated complex. The internal rotations, taken into consideration in this work, are responsible for an increase of the preexponential factor by a factor of 6 in the forward reaction. The corrections are substantial and bring the theoretical predictions closer to the experimental estimates. A further increase of the frequency factor can be expected if a more elaborate treatment of the coupled internal rotations is performed. This extended model allows all stable conformers of all species in play to contribute to the equilibrium constant, $K_C^{\ddagger}$, of the reaction on an equal and correct footing. Hence, additional pathways towards reaction are taken into consideration. This extension is in progress.

On the other hand, for the reverse reaction the effect of considering internal rotations is very small. This is probably due to the similar structures of the product and the activated complex.

Especially when several reactions are taking place simultaneously and hence the deduction of experimental information on individual processes is extremely difficult, calculations can give a valuable contribution on the condition that the theoretical methods used are accurate enough for the problem under study. When the type of calculation presented here is repeated for other reactions of the complex coke formation network, it can give more insight into the relative importance of competing pathways. In particular, we plan to study one of the reactions leading to a further growth of the coke layer, namely, the cyclization of a primary butylbenzene radical. Calculated kinetic values of the cyclization process together with the results presented here enable us to validate on a theoretical basis some main assumptions of the kinetic model describing coke formation. This work is in progress.

Acknowledgment. This work is supported by the Fund for Scientific Research—Flanders (FWO) and the Research Board of Ghent University. Comments of the two reviewers are greatly appreciated.

Appendix

Procedure for Obtaining the Energy Levels of the Internal Rotations. The energy levels corresponding to one of the decoupled internal rotations (see eq 4) are the eigenvalues ϵ of the Schrödinger equation,

$$-\frac{\hbar^2}{2I}\psi''(\phi) + V(\phi)\psi(\phi) = \epsilon\psi(\phi)$$

where the wave function should obey the periodic boundary conditions $\psi(-\pi) = \psi(\pi)$ and $\psi'(-\pi) = \psi'(\pi)$.

Because the potential $V(\phi)$ is an even function of the rotation angle ϕ, the eigenfunctions will also be either even or odd, and the ϕ interval can be restricted to $[0,\pi]$.

We introduce N equidistant grid points $\phi_i = (i - {}^1/_2)\Delta$, where $i = 1, ..., N$ and $\Delta = \pi/N$. The values of ψ on the grid points are treated as discrete variables $\psi_i = \psi(\phi_i)$. Using finite differences, the second-order derivatives of ψ can be written in terms of ψ_i as

$$\psi''(\phi_i) = (\psi_{i+1} - 2\psi_i + \psi_{i-1})/\Delta^2$$

up to terms of first order in Δ. For the endpoints of the interval, we can use the odd or even character of the ψ:

$$\psi''_e(\phi_1) = (\psi_2 - \psi_1)/\Delta^2 \qquad \psi''_o(\phi_1) = (\psi_2 - 3\psi_1)/\Delta^2$$

$$\psi''_e(\phi_N) = (\psi_{N-1} - \psi_N)/\Delta^2 \qquad \psi''_o(\phi_1) = (\psi_{N-1} - 3\psi_N)/\Delta^2$$

This will automatically result in the correct boundary conditions for the odd and even solutions, $\psi'_e(0) = 0$ and $\psi'_e(\pi) = 0$ or $\psi_o(0) = 0$ and $\psi_o(\pi) = 0$.

By an evaluation of the Schrödinger equation on the N grid points, the problem is transformed to that of finding the eigenvalues of a symmetric and tridiagonal $N \times N$ matrix $T_{ij} = a_i\delta_{ij} + b(\delta_{i,j-1} + \delta_{j,i-1})$, where $b = -\hbar^2/(2I\Delta^2)$, $a_i = [\hbar^2/(2I\Delta^2)]n_i + V(\phi_i)$. For the even solutions, $n_1 = n_N = 1$; for the odd solutions $n_1 = n_N = 3$, whereas $n_i = 2$ for $i \neq 1, N$.

Finding the lowest eigenvalues of T can be done efficiently by exploiting the well-known Sturm−Liouville property of tridiagonal matrices. By definition of an integer function $M(\epsilon)$ as the number of negative values c_i in the recurrence

$$c_i = a_i - \epsilon - (b^2/c_{i-1})$$

where $i = 1, ..., N$ and $c_0 = 1$, it can be shown that $M(\epsilon)$ equals the number of eigenvalues of T that are smaller than ϵ. Bisection can then be used to find the eigenenergies ϵ_i where $M(\epsilon)$ is increased by m units (m being equal to the degeneracy of the eigenvalue).

As the number N of grid points is increased, the lowest eigenvalues of T converge to the true lowest eigenvalues of the Schrödinger equation. Typically, we used about 4000 grid points. We checked that this is sufficient to guarantee convergence of the rotational partition functions needed.

References and Notes

(1) Clymans, P. J.; Froment, G. F. *Comput. Chem. Eng.* **1984**, *8*, 137−142.

(2) Reyniers, G. C.; Froment, G. F.; Kopinke, F. D.; Zimmerman, G. *Ind. Eng. Chem. Res.* **1994**, *33* (11), 2584−2590.

(3) Plehiers, P. M.; Reyniers, G. C.; Froment, G. F. *Ind. Eng. Chem. Res*. **1990**, *29*, 636−641.

(4) Eyring, H. *J. Chem. Phys*. **1935**, 107. A more comprehensive treatment can be found in Wynne-Jones, W. F. K.; Eyring, H. *J. Chem. Phys.* **1935**, *3*, 492. This article is reproduced in full in Back, M. H.; Laidler, K. L. *Selected readings in chemical kinetics*; Pergamon: Oxford, 1967.

(5) Evans, M. G.; Polanyi, M. *Trans. Faraday Soc*. **1935**, *31*, 875; **1937**, *33*, 448.

(6) Laidler, K. J. *Chemical kinetics*; HarperCollins Publishers: New York, 1987.

(7) McQuarrie, D. A.; Simon, J. D. *Physical Chemistry−A molecular approach*; University Science Books: Sausalito, CA, 1997.

(8) For reviews, see, for example: (a) Pechukas, P. *Dynamics of Molecular Collisions, Part B*; Miller, W. H., Ed.; Plenum Press: New York, 1976. (b) Laidler, K. J.; King, M. C. *J. Phys. Chem.* **1983**, *87*, 2657. (c) Truhlar, D. G.; Hase, W. L.; Hynes, J. T. *J. Phys. Chem.* **1983**, *87*, 2664. (d) Gilbert, R. G.; Smith, S. C. *Theory of Unimolecular and Recombination Reactions*; Blackwell: Oxford, 1990.

(9) Willems, P. A.; Froment, G. F. *Ind. Eng. Chem. Res.* **1988**, *27*, 1959−1966.

(10) Willems, P. A.; Froment, G. F. *Ind. Eng. Chem. Res.* **1988**, *27*, 1966−1971.

(11) Benson, S. W. *Thermochemical kinetics*; John Wiley & Sons Inc.: New York, 1976.

(12) Heuts, J. P. A.; Gilbert, R. G.; Radom, L. *J. Phys. Chem.* **1996**, *100*, 18997−19006.

(13) Heuts, J. P. A.; Gilbert, R. G.; Radom, L. *Macromolecules* **1995**, *28*, 8771−8781.

(14) Smith, D. M.; Nicolaides, A.; Golding, B. T.; Radom, L. *J. Am. Chem. Soc.* **1998**, *120*, 10223−10233.

(15) Ayala, P. Y.; Schlegel, H. B. *J. Chem. Phys*. **1998**, *108*, 2314.

(16) East, A. L. L.; Radom, L. *J. Chem. Phys*. **1997**, *106*, 6655.

(17) Pitzer, K. S.; Gwinn, W. D. *J. Chem. Phys*. **1942**, *10*, 428−439.

(18) Kilpatrick, J. E.; Pitzer, K. S. *J. Chem. Phys.* **1949**, *17* (11), 1064−1075.

(19) Lister, D. G.; MacDonald, J. N.; Owen, N. L. *Internal Rotation and Inversion*; Academic Press Inc. (London) Ltd.: London, 1978. Kroto, H. W. *Molecular Spectra*; Dover Publications: New York, 1992.

(20) Frisch, M. J.; Trucks, G. W.; Schlegel, H. B.; Scuseria, G. E.; Robb, M. A.; Cheeseman, J. R.; Zakrzewski, V. G.; Montgomery, J. A., Jr.; Stratmann, R. E.; Burant, J. C.; Dapprich, S.; Millam, J. M.; Daniels, A. D.; Kudin, K. N.; Strain, M. C.; Farkas, O.; Tomasi, J.; Barone, V.; Cossi, M.; Cammi, R.; Mennucci, B.; Pomelli, C.; Adamo, C.; Clifford, S.; Ochterski, J.; Petersson, G. A.; Ayala, P. Y.; Cui, Q.; Morokuma, K.; Malick, D. K.; Rabuck, A. D.; Raghavachari, K.; Foresman, J. B.; Cioslowski, J.; Ortiz, J. V.; Stefanov, B. B.; Liu, G.; Liashenko, A.; Piskorz, P.; Komaromi, I.; Gomperts, R.; Martin, R. L.; Fox, D. J.; Keith, T.; Al-Laham, M. A.; Peng, C. Y.; Nanayakkara, A.; Gonzalez, C.; Challacombe, M.; Gill, P. M. W.; Johnson, B. G.; Chen, W.; Wong, M. W.; Andres, J. L.; Head-Gordon, M.; Replogle, E. S.; Pople, J. A. *Gaussian 98*, revision A.7; Gaussian, Inc.: Pittsburgh, PA, 1998.

(21) For an example of a reference work, see: Parr, R. G.; Yang, W. *Density-Functional Theory of Atoms and Molecules*; Oxford University Press: New York, 1989.

(22) Becke, A. D. *J. Chem. Phys*. **1993**, *98*, 5648.

(23) Krishnan, R.; Binkley, J. S.; Seeger, R.; Pople, J. A. *J. Chem. Phys*. **1980**, *72*, 650.

(24) Wong, M. W.; Radom, L. *J. Phys. Chem. A* **1998**, *102*, 2237−2245.

(25) Parker, C. L.; Cooksy, A. L. *J. Phys. Chem. A* **1998**, *102*, 6186−6190.

(26) Lynch, B. J.; Fast, P. L.; Harris, M.; Truhlar, D. G. *J. Phys. Chem. A* **2000**, *104*, 4811−4815.

(27) Ochterski, J. W.; Petersson, G. A.; Montgomery, J. A. *J. Chem. Phys*. **1996**, *104*, 2598−2619.

(28) Curtiss, L. A.; Raghavachari, K.; Trucks, G. W.; Pople, J. A. *J. Chem. Phys*. **1991**, *94*, 7221−7230.

(29) Mayer, P. M.; Parkinson, C. J.; Smith, D. M.; Radom, L. *J. Chem. Phys*. **1998**, *108*, 604−615.

(30) Peng, C.; Ayala, P. Y.; Schlegel, H. B.; Frisch, M. J. *J. Comput. Chem*. **1996**, *17*, 49.

(31) Peng, C.; Schlegel, H. B. *Isr. J. Chem*. **1994**, *33*, 449.

(32) Scott, A. P.; Radom, L. *J. Phys. Chem.* **1996**, *100*, 16502−16513.

(33) Hehre, W, J.; Radom, L.; Schleyer, P. v. R.; Pople, J. A. *Ab initio molecular orbital theory*; John Wiley & Sons: New York, 1986.

(34) Dickinson, J. A.; Joireman, P. W.; Kroemer, R. T.; Roberson, E. G.; Simons, J. P. *J. Chem. Soc., Faraday Trans*. **1997**, *93* (8), 1467−1472.

(35) Kerr, J. A.; Parsonage, M. J. *Evaluated Kinetic Data on Gas Phase addition reactions*: *Reactions of atoms and radicals with alkenes, alkynes and aromatic compounds*; Butterworths: London, 1972. Watkins, K. W.; O'Deen, L. A. *J. Phys. Chem.* **1969**, *73*, 4094−4102. Morganroth, W. E.; Calvert, J. G. *J. Am. Chem. Soc.* **1966**, *88*, 5387. Kerr, J. A.; Trotman-Dickenson, A. F. *J. Chem. Soc*. **1960**, 1611.

(36) Knyazev, V. D.; Slagle, I. R. *J. Phys. Chem.* **1996**, *100*, 5318−5328. Marshall, R. M. *Int. J. Chem. Kinet.* **1990**, *22*, 935. Gierczak, T.; Gawlowski, J.; Niedzielski, J. *React. Kinet. Catal. Lett*. **1988**, *36*, 435. Dean, A. D. *J. Phys. Chem.* **1985**, *89*, 4600. Warnatz, J. *Combustion Chemistry*; Gardiner, W. C., Jr., Ed.; Springer-Verlag: New York, 1984; p 197. Morganroth, W. E.; Calvert, J. G. *J. Am. Chem. Soc.* **1966**, *88*, 5387.